a nonlinear resistor having the same characteristic. Moreover, Lur'e systems have been intensively studied for a long time (see [Khalil, 2002] and references therein), since their structure emerges in several control problems and it is enjoyed by many well-known circuits (e.g. Duffing, Van der Pol). This suggests that it is possible to derive other conditions ensuring that memristor circuits are nonoscillatory. For instance, one possibility consists in exploiting the sufficient condition given in [Ofir *et al.*, 2024] for 2-contraction of Lur'e systems.

Remark 3.6. Theorem 1 can be used even if the memristor characteristic does not satisfy the slope-bounded condition on the real axis but only on some subset $[\xi_m, \xi_M]$. In this case, if (37) holds for some positive definite P, then oscillatory and more complex behaviors are not displayed in the region of the circuit state space delimited by the two hyperplanes $\xi = \xi_m$ and $\xi = \xi_M$.

4. Application Examples

In this section, Theorem 1 is first applied to the Chua's memristor circuit of Fig. 2 and then to the RLC-memristor circuit of Fig. 3.

4.1. *The Chua's memristor circuit*

By introducing the adimensional positive parameters $\alpha = C_2/C_1$ and $\beta = R^2C_2/L$ and rescaling the time t by the factor $1/(RC_2)$, the matrices (12) can be rewritten as

$$A = \begin{pmatrix} -\alpha & \alpha & 0 \\ 1 & -1 & 1 \\ 0 & -\beta & 0 \end{pmatrix}, \quad B = \begin{pmatrix} R\alpha \\ 0 \\ 0 \end{pmatrix}, \quad C = (1 \quad 0 \quad 0), \tag{41}$$

while $N(\xi)$ is any $\mathcal{C}^1$ function satisfying the slope-bounded condition (35) with $k_1 = m_0$ and $k_2 = m_1$ and such that $N(0) = 0$. We recall that the canonical piecewise-linear characteristic in (10) is not of class $\mathcal{C}^1$ but it can be arbitrarily approximated by suitable smooth-piecewise functions [Jimenez-Fernandez *et al.*, 2016]. It follows that the system Jacobian satisfies (36) with

$$A - k_i BC = \begin{pmatrix} -\alpha(1 + Rm_i) & \alpha & 0 \\ 1 & -1 & 1 \\ 0 & -\beta & 0 \end{pmatrix}, \quad i = 1, 2. \tag{42}$$

Our aim is to find regions on the (α, β)-plane where the Chua's memristor circuit is nonoscillatory by exploiting Theorem 1. We find it convenient to choose $m_0 = -0.8$, $m_1 = -0.5$, and $R = 1/0.7$, which are exactly the values considered in the celebrated Chua's circuit where the two-terminal element **L**, whose impedance is given by

$$G(s) = C(sI_3 - A)^{-1}B = R\frac{\alpha(s^2 + s + \beta)}{s^3 + (1+\alpha)s^2 + \beta s + \alpha\beta},$$

is connected to a nonlinear resistor described in the voltage–current domain by the relation $i_{\mathbf{L}} = -N_{pwl}(v_{\mathbf{L}})$. The dynamics of this circuit has been thoroughly analyzed in [Chua *et al.*, 1986]. The circuit has three equilibrium points for all positive α and β and it displays oscillatory, mono-scroll and double-scroll chaotic attractors in the region

$$\Lambda_O = \left\{ \alpha > 0, \beta > 0 : \beta \leq \beta_C = \frac{5}{7}\alpha + \frac{10}{49}\alpha^2 \right\}, \tag{43}$$

where $\beta = \beta_C$ is the Hopf bifurcation curve. According to Remark 3.5, this suggests that the region in the (α, β)-plane where the memristor circuit is nonoscillatory does not intersect Λ_O. Indeed, it is disjoint from all the regions where the circuit displays either oscillations or more complex behaviors for any memristor characteristic satisfying (35) with $k_1 = -0.8$ and $k_2 = -0.5$.

By substituting $m_0 = -0.8$, $m_1 = -0.5$, and $R = 1/0.7$ in (42), we have that

$$A - k_1 BC = \begin{pmatrix} \frac{\alpha}{7} & \alpha & 0 \\ 1 & -1 & 1 \\ 0 & -\beta & 0 \end{pmatrix},$$

$$A - k_2 BC = \begin{pmatrix} -\frac{2\alpha}{7} & \alpha & 0 \\ 1 & -1 & 1 \\ 0 & -\beta & 0 \end{pmatrix}.$$

As a consequence, the relative 2-additive compound matrices read

$$(A - k_1 BC)^{[2]} = \begin{pmatrix} \frac{\alpha}{7} - 1 & 1 & 0 \\ -\beta & \frac{\alpha}{7} & \alpha \\ 0 & 1 & -1 \end{pmatrix},$$

$$(A - k_2 BC)^{[2]} = \begin{pmatrix} -\frac{2\alpha}{7} - 1 & 1 & 0 \\ -\beta & -\frac{2\alpha}{7} & \alpha \\ 0 & 1 & -1 \end{pmatrix}.$$

According to Remark 3.3, condition (37) is fulfilled only if $(A - kBC)^{[2]}$ are Hurwitz matrices for all $k \in [-0.8, -0.5]$. Tedious though straightforward computations lead to show that these matrices are Hurwitz if and only if α and β belong to the following region:

$$\Lambda_H = \left\{ \alpha > 0, \beta > 0 : \right.$$
$$\left. \alpha < \frac{7}{2}, \beta \geq \beta_H = \frac{\frac{2\,\alpha^3}{343} - \frac{2\alpha^2}{7} + 2\alpha - 2}{1 - \frac{2\alpha}{7}} \right\}. \quad (44)$$

Clearly, Λ_H must contain the nonoscillatory region we are looking for. To obtain this region for $\alpha \in (0, 2.5)$, we compute the values of β such that condition (37), i.e.

$$(A - k_i BC)^{[2]^\top} P + P(A - k_i BC)^{[2]} < 0, \quad i = 1, 2, \quad (45)$$

is feasible for some symmetric positive definite $P_2 \in \mathbb{R}^{3\times 3}$. This feasibility problem is solved via the software Yalmip [Lofberg, 2004], obtaining the region depicted in green in Fig. 5 which is unbounded above. Hence, the circuit does not display oscillatory and more complex attractors for any α and β belonging to this region and any memristor characteristic such that $N(0) = 0$ and condition (35) holds for $k_1 = -0.8$ and $k_2 = -0.5$. Figure 5(a) confirms that the nonoscillatory region is contained in the region Λ_H which is bounded from below by the curve $\beta = \beta_H$ (marked black), while Fig. 5(b) shows that there is some gap between the nonoscillatory region and the region Λ_O.

According to Remark 3.4, this gap can be reduced by using an HPLF of fourth order ($m = 2$) instead of the quadratic one. In this case, we have to find a symmetric positive definite $P_2 \in \mathbb{R}^{6\times 6}$ and $\gamma \in \mathbb{R}^6$ solving condition (40), i.e.

$$(A - k_i BC)_{\{2\}}^{[2]^\top} P_2 + P_2 (A - k_i BC)_{\{2\}}^{[2]} + L(\gamma) < 0, \quad i = 1, 2, \quad (46)$$

where $(A - k_i BC)_{\{2\}}^{[2]} \in \mathbb{R}^{6\times 6}$, $i = 1, 2$, are the extended matrices of $(A - k_i BC)^{[2]}$ with $m = 2$ and

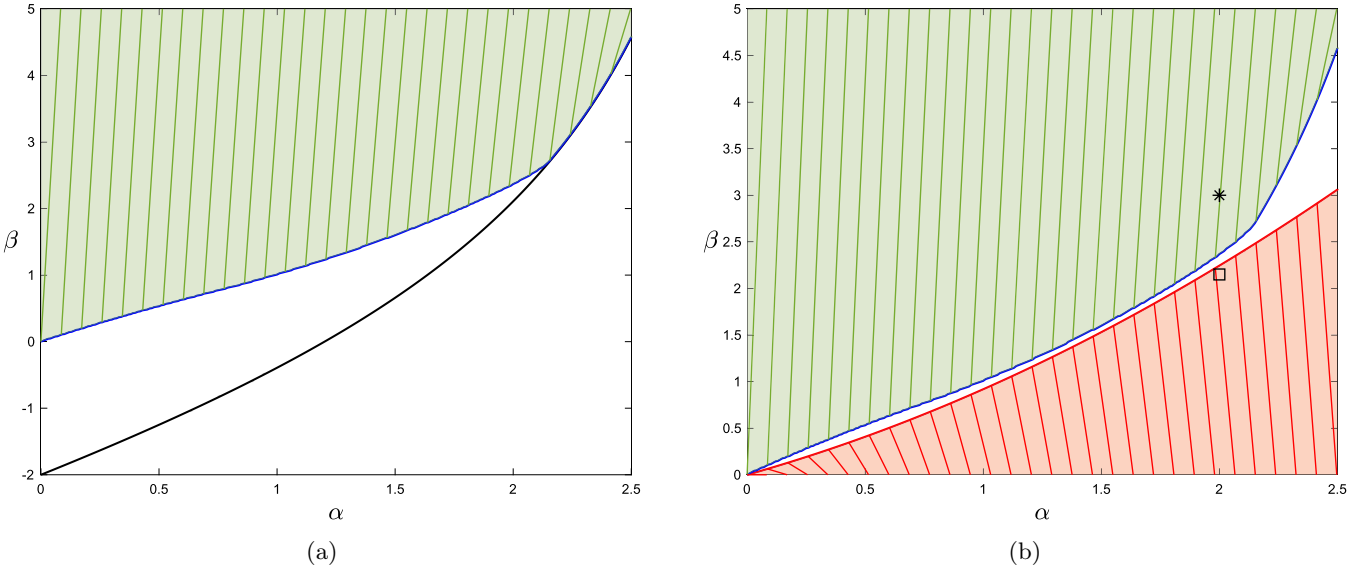

Fig. 5. Regions of the (α, β) plane: (a) Nonoscillatory region (green) and region Λ_H bounded from below by the black curve ($\beta = \beta_H$); (b) nonoscillatory region (green) and region Λ_O (red). The simulations in Figs. 7 and 8 refer to the point $(\alpha, \beta) = (2, 3)$ (marked with $\star$), while those in Fig. 9 to $(\alpha, \beta) = (2, 2.3)$ (marked with $\square$).

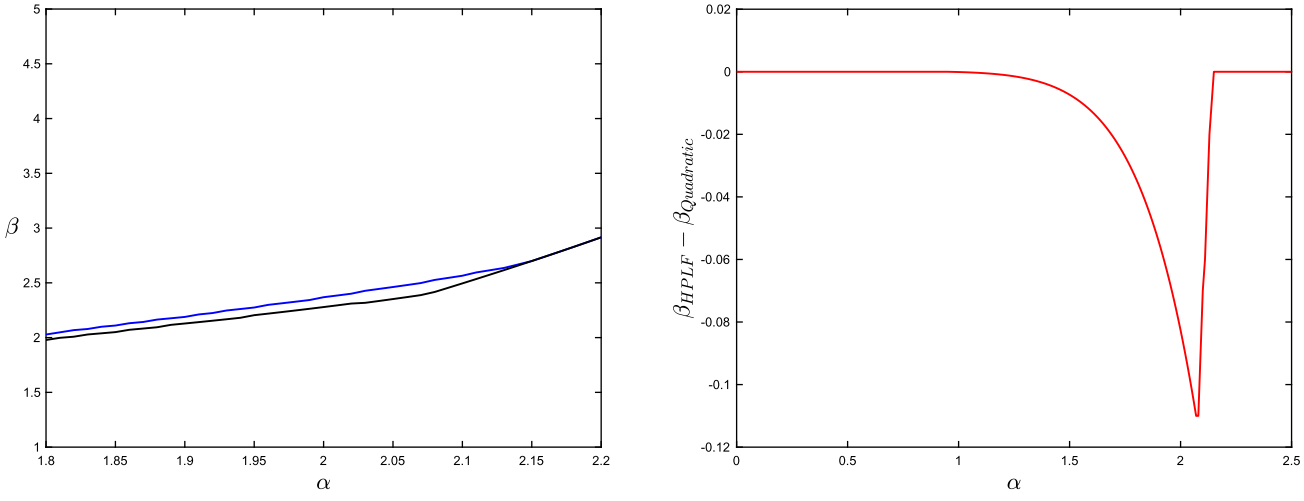

(a) (b)

Fig. 6. (a) Curves that are bounded from below the nonoscillatory regions obtained via (45) (blue) and (46) (black) for $\alpha \in [1.8, 2.2]$. (b) Difference between the two curves.

$L(\gamma)$ reads

$$L(\gamma) = \begin{pmatrix} 0 & 0 & -\gamma_1 & 0 & -\gamma_2 & \gamma_4 \\ 0 & 2\gamma_1 & 0 & \gamma_2 & -\gamma_3 & -\gamma_5 \\ -\gamma_1 & 0 & 0 & \gamma_3 & 0 & -\gamma_6 \\ 0 & \gamma_2 & \gamma_3 & 2\gamma_4 & \gamma_5 & 0 \\ -\gamma_2 & -\gamma_3 & 0 & \gamma_5 & 2\gamma_6 & 0 \\ -\gamma_4 & -\gamma_5 & -\gamma_6 & 0 & 0 & 0 \end{pmatrix}.$$

By solving the feasibility problem (46) via the software Yalmip [Lofberg, 2004], a slightly larger nonoscillatory region is obtained. Figure 6(a) shows the curves that are bounded from below the two nonoscillatory regions in the interval $\alpha \in [1.8, 2.2]$ where the difference is more significant, while Fig. 6(b) displays the difference between the lower bounds of β obtained via the HPLF with $m = 2$ and the quadratic function. Hence, we can argue that in this case, the quadratic Lyapunov function does not seem to provide a conservative result with respect to the use of HPLFs.

Finally, we analyze the dynamics of the Chua's memristor circuit with $R = 1/0.7$, $C_1 = 1$, $C_2 = 2$, $L = 1.36$ and the canonical piecewise-linear characteristic in (10) approximated via a smooth-piecewise function as shown in [Jimenez-Fernandez *et al.*, 2016]. With this choice, the invariant manifolds in (14) boil down to

$$\mathcal{M}_{\mathcal{I}} = \{(v_{C_1}, v_{C_2}, i_L)^\top \in \mathbb{R}^3, \varphi_M \in \mathbb{R} : \varphi_M + 0.5 v_{C_1} + 0.33 i_L + 1.43 N(\varphi_M) = \mathcal{I}\},$$

while we have that $\alpha = 2$ and $\beta = 3$, which corresponds to the point of the nonoscillatory region marked with $\star$ in Fig. 5(b). Figures 7 and 8 display the dynamical behaviors on the invariant manifold $\mathcal{M}_{\mathcal{I}}$ with $\mathcal{I} = 0$ and $\mathcal{I} = \pm 2$. The manifold has three equilibrium points (two stable and one unstable) for $\mathcal{I} = 0$ and a unique stable equilibrium point for $\mathcal{I} = \pm 2$. As expected, periodic solutions are not displayed and all the trajectories show convergence

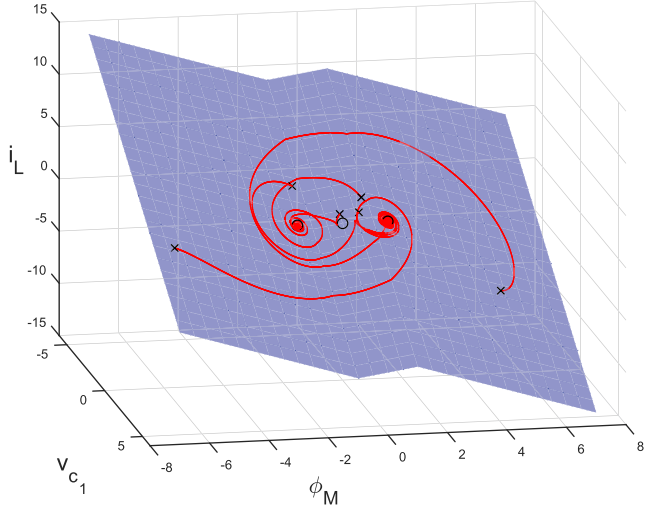

Fig. 7. State space trajectories of the Chua's memristor circuit projected on the subspace with $R = 1/0.7$, $C_1 = 1$, $C_2 = 2$, $L = 1.36$ [corresponding to the point marked with $*$ in Fig. 5(b)] and $N(\varphi_M)$ being a smooth-piecewise approximation of $N_{pwl}(\varphi_M)$. The initial conditions (marked with $\times$) are chosen to ensure that the trajectories lie on the invariant manifolds $\mathcal{M}_{\mathcal{I}}$ with $\mathcal{I} = 0$. The three equilibrium points are marked with $\circ$.